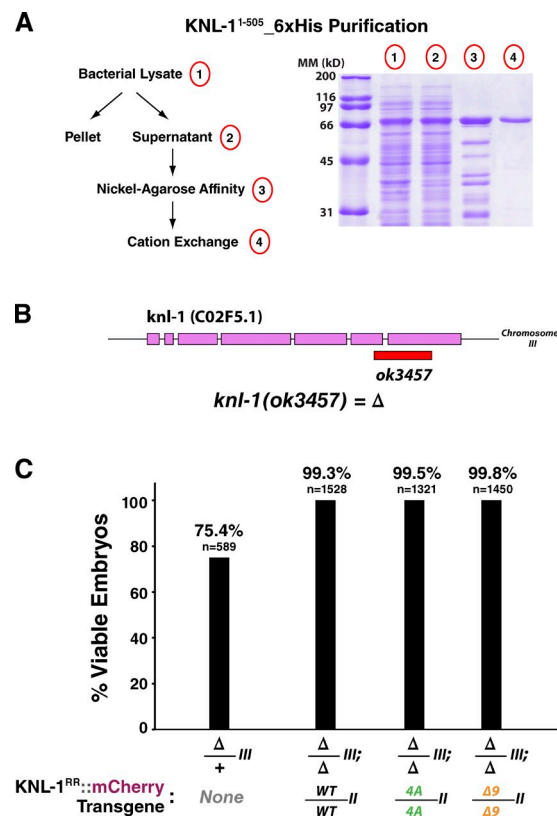
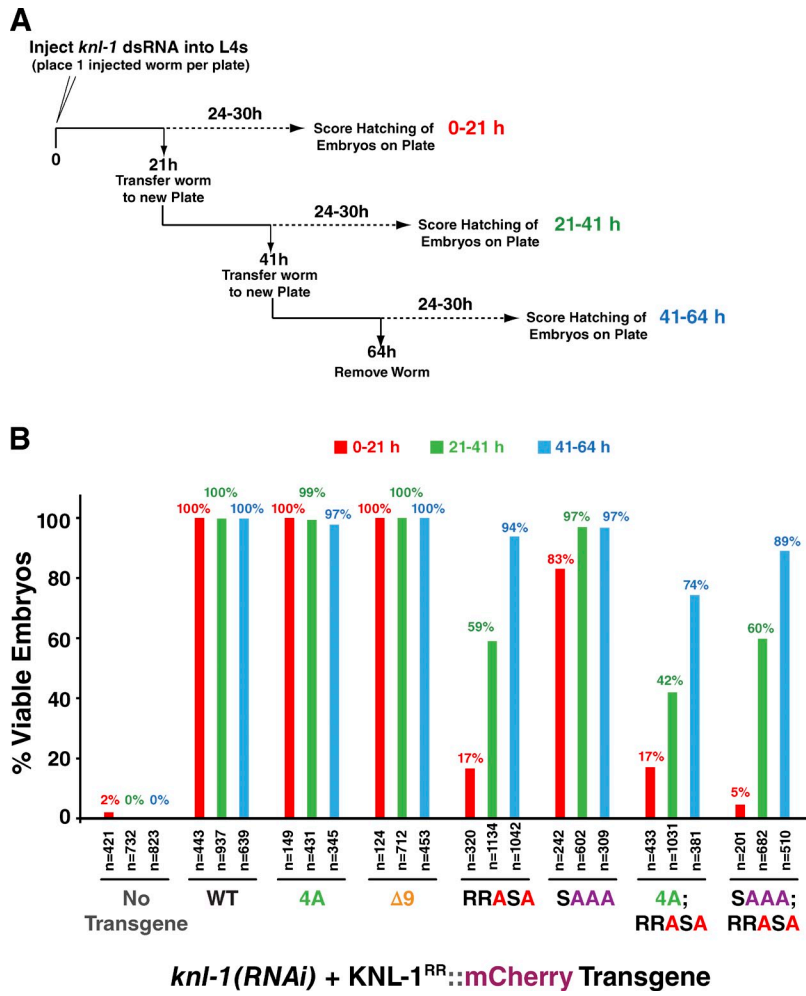


Espeut et al., <http://www.jcb.org/cgi/content/full/jcb.201111107/DC1>

**Figure S1. KNL-1<sup>1-505</sup> purification and analysis of rescue of the lethality of the *knl-1(ok3457)* deletion mutant by KNL-1 mutants.** (A) Purification of KNL-1<sup>1-505</sup>-6xHis from bacteria using nickel agarose affinity and cation exchange chromatography. Each step of the purification was analyzed by SDS-PAGE and Coomassie blue staining. MM, molecular mass. (B) A schematic representation of the deletion mutant *knl-1(ok3457)*. The red box indicates the region deleted from the *knl-1* locus. KNL-1 is a 1,010-amino acid protein encoded by seven exons. The *ok3457* allele inserts the sequence 5'-GGAAATTGAAAATGGCTGAA-3' after the *knl-1* sequence 5'-GAATGGGCAAACATGGAAAGCTGACAGA-3' in exon 6; this insertion is followed by a deletion of 602 base pairs before the *knl-1* sequence 5'-AGCTAAGAGGTCTCGATAAGATGGCTGTC-3'. The insertion/deletion introduces a frame shift after amino acid 721, which deletes the last 289 amino acids of KNL-1 and predicts the insertion of the extra amino acids TEEIRKWLKAKRSR following amino acid 721. (C) Embryo viability of the *knl-1(ok3457)* deletion mutant in the presence of the WT, 4A, and Δ9 KNL-1<sup>RR</sup>::mCherry transgenes. The *knl-1* locus is on chromosome III, and transgenes are inserted on chromosome II. As a first step, N2 (WT) males were crossed to the balanced *knl-1(ok3457)* deletion mutant, and heterozygous worms were singled onto plates. Viability of embryos laid by worms heterozygous for the *knl-1(ok3457)* mutant allele was quantified; heterozygosity of the mother was confirmed by PCR. 25% of the progeny embryos of heterozygous worms was inviable, and homozygous *knl-1(ok3457)* deletion mutant worms were never recovered, indicating that the *ok3457* allele is recessive embryonic lethal. Next, males from the three KNL-1 transgenic strains (WT, 4A, and Δ9) were crossed into the *knl-1(ok3457)* deletion. In all three cases, after three generations, homozygous *knl-1(ok3457)* deletion mutants harboring homozygous transgene insertions were recovered. Progeny tests on these rescued mutant lines revealed no significant embryonic lethality, as depicted in the graph.

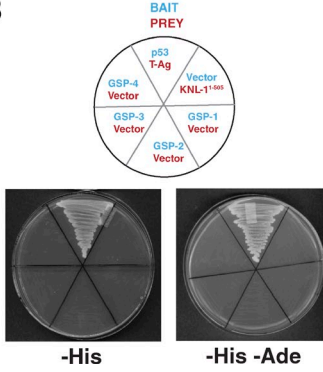


**Figure S2. Embryonic viability at different time points after dsRNA injection for engineered KNL-1 mutants.** (A) A schematic of the experimental procedure used to assess the effect of mutations engineered in KNL-1 on embryonic viability. (B) Results of the viability assay described in A. In this assay, late L4-stage worms were injected with dsRNA-targeting endogenous *knl-1*, and the embryos laid by the injected worms were collected over the indicated time intervals and scored for viability (as assessed by their hatching to form larvae). The RNAi response triggered by the introduction of dsRNA leads to rapid degradation of the target mRNA in the germline of the animal. As the injected worms mature into young adults, they start fertilizing oocytes and making embryos. The process of embryo production progressively depletes the target protein that was already present in the germline at the time of injection so that by 12–24 h after injection, newly formed embryos are significantly depleted of maternally deposited protein. This depletion of maternally contributed protein persists over the time course of the experiment and typically becomes more penetrant over time, with the maternal load >95% depleted of the target protein 36–48 h after injection. Maternally loaded protein is thought to control the first five to seven rounds of cell division, after which proteins produced in the embryo (zygotic expression from the embryo's genome) become progressively more important. During the early postinjection time window (0–21 h), the embryos produced by the injected worms receive a relatively large dose of dsRNA (this is because the injected dsRNA is expelled out of the gonad via embryo production), which is able to also reduce embryonic (zygotic) gene expression. All embryos produced by worms injected with *knl-1* dsRNA that lacked an RNAi-resistant transgene were inviable over all assayed postinjection intervals because inhibition of *knl-1* during either the early or late embryonic divisions results in catastrophic chromosome missegregation. In contrast, embryos with RNAi-resistant transgenes encoding WT KNL-1 or the 4A and Δ9 microtubule-binding activity mutations did not show any significant lethality at any time point, suggesting that KNL-1 with these mutations can support chromosome segregation and embryonic development with sufficient fidelity to maintain viability. Embryos produced by worms injected with *knl-1* dsRNA that harbored RNAi-resistant transgenes encoding KNL-1 with the RRASA mutation either alone or in combination with the SAAA or 4A mutations showed partial embryonic lethality and whose magnitude decreased with time after injection. This result suggests that depletion of endogenous KNL-1 in the maternal load alone (most penetrant at late time points) does not lead to penetrant lethality of embryos expressing KNL-1 with the RRASA mutation. However, higher penetrance lethality is observed for the brood of embryos produced during the early time interval because the functionality of the RRASA mutant KNL-1 is being assayed across both the early embryonic and subsequent zygotic divisions. This early time window high lethality can therefore be interpreted as a consequence of cumulative low frequency defects in chromosome segregation throughout embryogenesis.

**A** *C. elegans* PP1c Subunits

	* * *	
GSP-1	1 -MSNDCLNLIDNLITRLLEVGCRCPKPTMSEAEIFALCHKSREIPLSQPI50	
GSP-2	1 -MDVEKLNLNLIDNLITRLLEVGCRCPKGNQLTSEIKLCLQKSRREIPLSQPI50	
GSP-3	1 -MTAPMDVNLMLMSRLLLNVGSGRLTTSVNEQEIQTCAVAKSVFASQSA549	
GSP-4	1 -MTAPMDVNLMLMSRLLLNVGSGRLTTSVNEQEIQTCAVAKSVFASQSA549	
Rat PP1c	1 MADIKLNLDNIDSLITRLLEVGCRCPKGNQLQEERCLCEIPLSQPI50	
	* *	
GSP-1	52 LLEELAFLK I CGDIHQYNDLRLRFIFYGCFPPESNYLFLGQYVDRGKQSLE102	
GSP-2	51 LLEELAFLK I CGDVHQYNDLRLRFIFYGCFPPESNYLFLGQYVDRGKQSLE101	
GSP-3	50 LLEELAFLK I VEGDIHQYNDLRLRFIFYGCFPPDVAFLFLGQYVDRGKQNIE100	
GSP-4	50 LLEELAFLK I VEGDIHQYNDLRLRFIFYGCFPPDVAFLFLGQYVDRGKQNIE100	
Rat PP1c	52 LLEELAFLK I CGDIHQYNDLRLRFIFYGCFPPESNYLFLGQYVDRGKQSLE102	
	* *	
GSP-1	103 TICLLLAAYKYPENFFLLRGHHHEASINRYIGYEDECKRKNY-IKLWKTFT152	
GSP-2	102 TICLLLAAYKYPENFFLLRGHHHEASINRYIGYEDECKRKNY-IKLWKTFT151	
GSP-3	101 TICMLLCFKKYPENFFLLRGHHHEAPINRYVGYTTECHRKYSTRLWSIF151	
GSP-4	101 TICMLLCFKKYPENFFLLRGHHHEASINRYIGYEDECKRKNY-IKLWKTFT151	
Rat PP1c	103 TICLLLAAYKYPENFFLLRGHHHEASINRYIGYEDECKRKNY-IKLWKTFT152	
	* *	
GSP-1	153 TDCFCNCLPAAFLK I FCHGGLSPDQWMEQIQRKVMPFTDVFOTGLCC0203	
GSP-2	152 TDCFCNCLPAAFLK I FCHGGLSPDQWMEQIIRRIMPFTDVFOTGLCC0202	
GSP-3	152 QDTFWNPMLCLLIGSRLLCMHGGELSPHLQTLDDQLPFDPDPFNSIGID202	
GSP-4	152 QDTFWNPMLCLLIGSRLLCMHGGELSPHLQTLDDQLPFDPDPFNSIGID202	
Rat PP1c	153 TDCFCNCLPAAFLK I FCHGGLSPDQWMEQIIRRIMPFTDVFOTGLCC0203	
	* *	
GSP-1	204 LLWSDPDKOYV DGCNDKQHVS-TCT DIVAKYLHHDLDL CRAHQVVEDC224	
GSP-2	203 LLWSDPDKOYV DGCNDKQHVS-TCT DIVAKYLHHDLDL CRAHQVVEDC223	
GSP-3	203 LLWADPQDWVKGWQANTGRGVVFTFGDVADVDCSRLDIDIVARAHQVQDG253	
GSP-4	203 LLWADPQDWVKGWQANTGRGVVFTFGDVADVDCSRLDIDIVARAHQVQDG253	
Rat PP1c	204 LLWSDPDKOYV DGCNDKQHVS-TCT DIVAKYLHHDLDL CRAHQVVEDC224	
	* *	
GSP-1	255 YEFFFAKSQLVLF SAPPNYCGEDFAACGMMVDEETLMESQFLKPKAKKYY305	
GSP-2	254 YEFFFAKSQLVLF SAPPNYCGEDFAACGMMVDEETLMESQFLKPKAKKYY304	
GSP-3	254 YEFFFAKSQLVLF SAPPHYCGQQFDNSAATMKVDEENMVCTFVWYKPTPKSLR-303	
GSP-4	254 YEFFFAKSQLVLF SAPPHYCGQQFDNSAATMKVDEENMVCTFVWYKPTPKSLR-303	
Rat PP1c	255 YEFFFAKSQLVLF SAPPNYCGEDFAACGAMMVDDEETLMESQFLKPKAKKYY304	

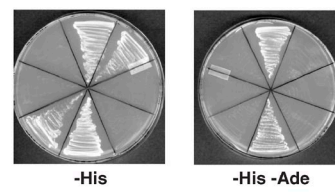
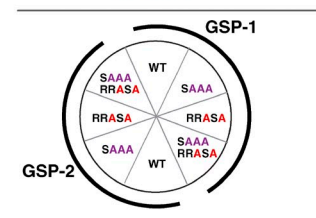
**B**



**Figure S3. PP1 catalytic subunit sequence alignments and controls for yeast two-hybrid analysis.** (A) Primary sequence alignment of the four PP1 catalytic (PP1c) subunits in *C. elegans*, GSP-1, -2, -3, and -4. Asterisks mark residues conserved between GSP-1, -2, and mammalian PP1c-γ, but divergent in GSP-3 and -4, that make direct contacts with the GILK motif of inhibitor 2 (Hurley et al., 2007). (B) Controls showing that the fusions tested in the yeast two-hybrid analysis (KNL-1<sup>1–505</sup>, GSP-1, -2, -3, or -4) do not autoactivate transcription of the reporter genes. (C) High stringency selection (-His and -Ade) reveals reduced growth of the SAAA mutant, indicating that the SILK motif contributes to the interaction of KNL-1 with GSP-1/2.

**C**

KNL-1<sup>FL</sup> (WT or Mutant) + GSP-1 or GSP-2



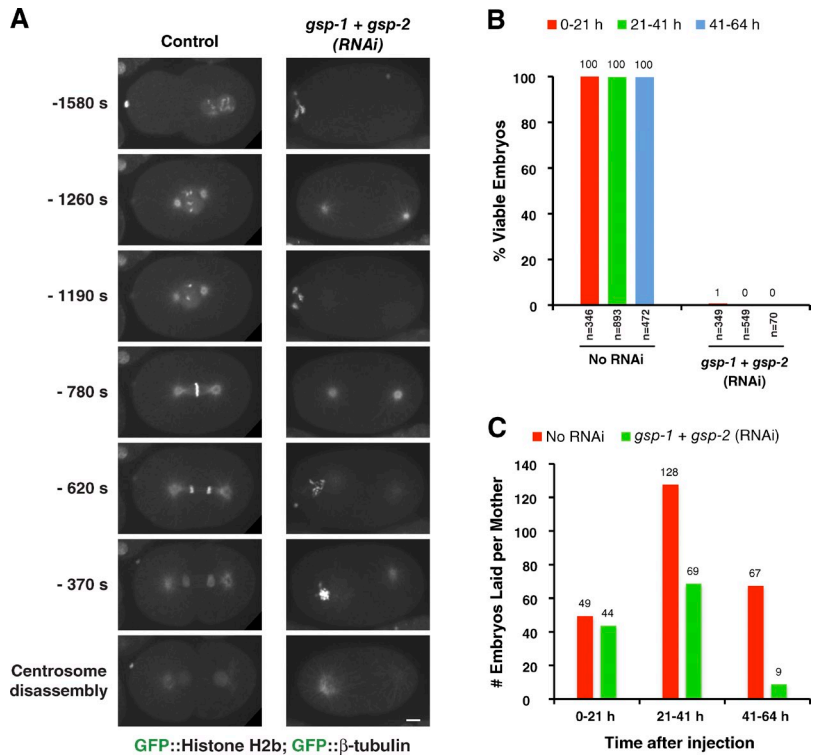


**Figure S4. Phenotype caused by depleting PP1 in *C. elegans* embryos.** (A) A still from time-lapse sequences of one-cell control or *gsp-1 + gsp-2(RNAi)* embryos expressing the indicated markers. *gsp-1 + gsp-2(RNAi)* embryos exhibited severe and pleiotropic defects, including oocyte meiosis problems, lack of recognizable mitotic chromosomes, and failure of spindle assembly. Sequences were time aligned using centrosome disassembly (which occurs during late anaphase/telophase in control embryos), as that was the only feature that could be scored in the *gsp-1 + gsp-2(RNAi)* embryos. Bar, 5  $\mu$ m. (B) Embryonic viability analysis conducted as in Fig. S2 B. (C) Brood size measurements. *gsp-1 + gsp-2(RNAi)* embryos exhibit a significantly reduced brood size, likely reflecting a function for PP1 in oocyte production in the germline.

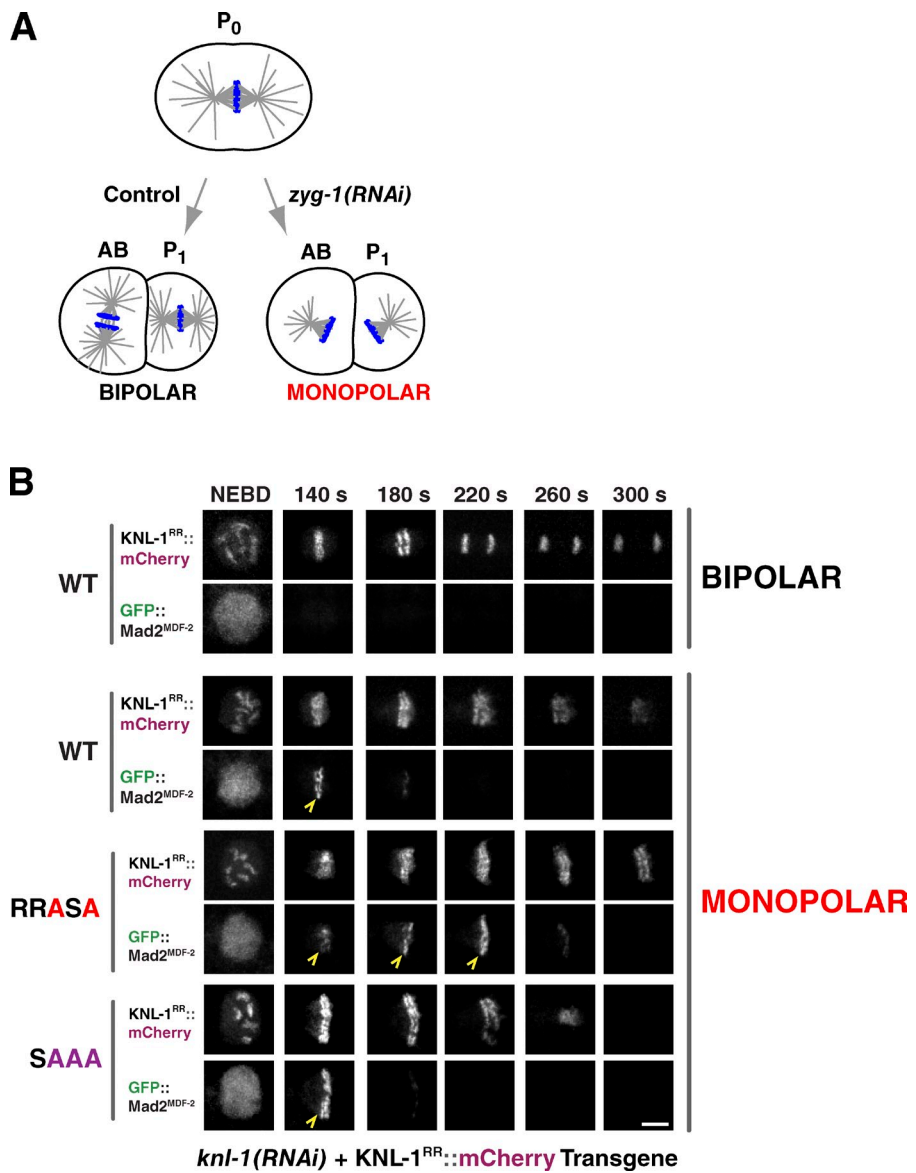
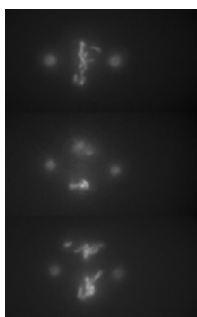
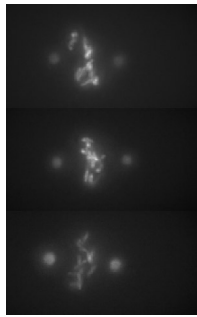


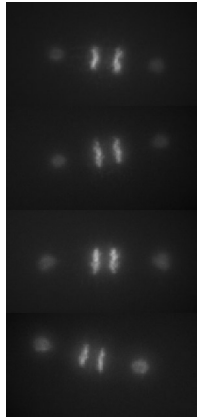
**Figure S5. PP1-binding mutants of KNL-1 significantly extend localization of Mad2<sup>MDF-2</sup> at unattached kinetochores of monopolar spindles.** (A) A schematic of the monopolar spindle-based checkpoint assay in *C. elegans* embryos. Depletion of the centrosome duplication kinase ZYG-1 is used to generate monopolar spindles in the second division, which trigger a spindle checkpoint-dependent cell cycle delay. (B) Stills from time-lapse sequences of the AB cell monopolar division in worm strains coexpressing GFP::Mad2<sup>MDF-2</sup> and the indicated transgenes. Mad2<sup>MDF-2</sup> accumulation on unattached kinetochores is marked with open arrowheads. Bar, 3  $\mu$ m.



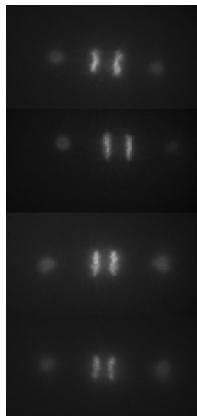
**Video 1. Rescue of *knl-1* depletion by a single-copy transgene insertion-encoded KNL-1<sup>RR</sup>::mCherry.** NEBD—anaphase interval in one-cell *C. elegans* embryos expressing GFP::histone H2b and GFP:: $\gamma$ -tubulin to mark chromosomes and spindle poles, respectively. The panels in the video from top to bottom show control (strain TH32), *knl-1(RNAi)*, and *knl-1(RNAi)* + WT KNL-1<sup>RR</sup>::mCherry. Each frame in the video is 10 s apart and is a maximum intensity projection of 5  $\times$  2- $\mu$ m z sections acquired using a deconvolution microscope (DeltaVision). Playback rate is 2 frames per second (20x real time). This video is related to Fig. 1.



**Video 2. Microtubule-binding mutants of KNL-1 do not affect formation of load-bearing attachments or chromosome segregation.** NEBD-anaphase interval in one-cell *C. elegans* embryos expressing GFP::histone H2b and GFP:: $\gamma$ -tubulin to mark chromosomes and spindle poles, respectively. The panels in the video show *knl-1(RNAi)* + KNL-1<sup>RR</sup>::mCherry transgenes WT, 4A, and  $\Delta$ 9 (the WT sequence is the same as in Video 1). Each frame in the video is 10 s apart and is a maximum intensity projection of 5  $\times$  2- $\mu$ m z sections acquired using a deconvolution microscope (DeltaVision). Playback rate is 2 frames per second (20x real time). This video is related to Fig. 2.



**Video 3. PP1-docking mutants of KNL-1 exhibit kinetic defects in load-bearing attachment formation.** NEBD-anaphase interval in one-cell *C. elegans* embryos expressing GFP::histone H2b and GFP:: $\gamma$ -tubulin to mark chromosomes and spindle poles, respectively. The panels in the video show *knl-1(RNAi)* + KNL-1<sup>RR</sup>::mCherry transgenes WT, SAAA, RRASA, and SAAA;RRASA (the WT sequence is the same as in Video 1). Each frame in the video is 10 s apart and is a maximum intensity projection of 5  $\times$  2- $\mu$ m z sections acquired using a deconvolution microscope (DeltaVision). Playback rate is 2 frames per second (20x real time). This video is related to Fig. 6.



**Video 4. Disrupting both microtubule-binding and PP1-docking activities of KNL-1 has an additive phenotype.** NEBD-anaphase interval in one-cell *C. elegans* embryos expressing GFP::histone H2b and GFP:: $\gamma$ -tubulin to mark chromosomes and spindle poles, respectively. The panels in the video show *knl-1(RNAi)* + KNL-1<sup>RR</sup>::mCherry transgenes WT, 4A, RRASA, and 4A;RRASA (the WT sequence is the same as in Video 1, and the 4A and RRASA sequences are same as in Video 3). Each frame in the video is 10 s apart and is a maximum intensity projection of 5  $\times$  2- $\mu$ m z sections acquired using a deconvolution microscope (DeltaVision). Playback rate is 2 frames per second (20x real time). This video is related to Fig. 7.

Table S1. Statistical analysis of NEBD-anaphase onset interval in one-cell embryos

	WT (mad-2 RNAi)	4A (mad-2 RNAi)	4A (mad-2 RNAi)	$\Delta 9$	$\Delta 9$ (mad-2 RNAi)	RRASA	RRASA (mad-2 RNAi)	SAAA	SAAA (mad-2 RNAi)	4A-RRASA	4A-RRASA (mad-2 RNAi)	SAAA- RRASA	SAAA- RRASA (mad-2 RNAi)
WT	0.5025	<0.0001	0.5045	<0.0001	0.1713	<0.0001	<0.0001	0.0040	0.0343	<0.0001	<0.0001	<0.0001	<0.0001
WT (mad-2 RNAi)		0.0001	0.2353	<0.0001	0.157	<0.0001	<0.0001	0.0075	0.0476	<0.0001	<0.0001	<0.0001	<0.0001
4A		0.0003	0.7299	0.0011	<0.0001	0.1529	0.0086	0.0058	<0.0001	0.0080	<0.0001	0.0442	
4A (mad-2 RNAi)			0.0002	0.6801	<0.0001	<0.0001	0.0594	0.2408	<0.0001	<0.0001	<0.0001	<0.0001	<0.0001
$\Delta 9$				0.0006	<0.0001	0.3068	0.0040	0.0031	<0.0001	0.0225	0.0002	0.1097	
$\Delta 9$ (mad-2 RNAi)					<0.0001	<0.0001	0.1559	0.4518	<0.0001	<0.0001	<0.0001	<0.0001	<0.0001
RRASA						<0.0001	<0.0001	<0.0001	<0.0001	0.0170	0.6525	<0.0001	
RRASA (mad-2 RNAi)							<0.0001	<0.0001	<0.0001	0.0998	0.0003	0.4882	
SAAA								0.5443	<0.0001	<0.0001	<0.0001	<0.0001	
SAAA (mad-2 RNAi)									<0.0001	<0.0001	<0.0001	<0.0001	
4A- RRASA										<0.0001	<0.0001	<0.0001	
4A- RRASA (mad-2 RNAi)											0.0351	0.2305	
SAAA- RRASA												0.0006	
SAAA- RRASA (mad-2 RNAi)													

Unpaired *t* tests were used to compare the measured intervals plotted in Figs. 1 K, 2 E, 6 E, and 7 E.

Table S2. Statistical analysis of monopolar spindle–induced cell cycle delay in two-cell embryos

	WT (zyg-1 RNAi)	4A	4A (zyg-1 RNAi)	$\Delta 9$	$\Delta 9$ (zyg-1 RNAi)	RRASA	RRASA (zyg-1 RNAi)	SAAA	SAAA (zyg-1 RNAi)	4A-RRASA	4A-RRASA (zyg-1 RNAi)	RRASA-SAAA	RRASA-SAAA (zyg-1 RNAi)
WT	<0.0001	0.0065	<0.0001	0.0067	<0.0001	<0.0001	<0.0001	0.0282	<0.0001	<0.0001	<0.0001	0.0010	<0.0001
WT (zyg-1 RNAi)		<0.0001	<0.0001	<0.0001	<0.0001	0.0010	<0.0001	<0.0001	0.3646	0.9719	<0.0001	0.1418	0.0002
4A			<0.0001	0.5132	<0.0001	0.0004	<0.0001	<0.0001	<0.0001	0.0063	<0.0001	0.0322	<0.0001
4A (zyg-1 RNAi)				<0.0001	0.7886	<0.0001	0.0178	<0.0001	<0.0001	<0.0001	0.0325	<0.0001	0.0854
$\Delta 9$					<0.0001	0.0077	<0.0001	<0.0001	<0.0001	0.0152	<0.0001	0.0811	<0.0001
$\Delta 9$ (zyg-1 RNAi)						<0.0001	0.0566	<0.0001	<0.0001	<0.0001	0.0613	<0.0001	0.0780
RRASA							<0.0001	<0.0001	0.0002	0.1176	<0.0001	0.7142	<0.0001
RRASA (zyg-1 RNAi)								<0.0001	<0.0001	0.0051	0.0027	<0.0001	0.9262
SAAA								<0.0001	0.0004	<0.0001	0.0011	<0.0001	
SAAA (zyg-1 RNAi)									0.7648	<0.0001	0.0601	0.0004	
4A-RRASA										<0.0001	0.3285	0.0024	
4A-RRASA (zyg-1 RNAi)											<0.0001	0.0021	
RRASA-SAAA												0.0002	
RRASA-SAAA (zyg-1 RNAi)													

Unpaired *t* tests were used to compare measured intervals [NEBD–decondensation in AB Cell] plotted in Figs. 3 B, 6 H, and 7 E.

Table S3. *C. elegans* strains used in this study

Strain no.	Genotype
N2	WT (ancestral N2 Bristol)
TH32	unc-119(ed3) III; ruls32 [pAZ132; pie-1/GFP::his-58; unc-119(+)] III; ddls6 [pie-1/GFP::tbg-1; unc-119(+)] V
OD334	unc-119(ed3) III; ltsi1 [pOD809/pJE110; Pknl-1::KNL-1 reencoded::mCherry; cb-unc-119(+)] II
OD413	unc-119(ed3) III; ltsi16 [pOD930/pJE156; Pknl-1::KNL-1 reencoded(4A)::mCherry; cb-unc-119(+)] II
OD415	unc-119(ed3) III; ltsi18 [pOD931/pJE157; Pknl-1::KNL-1 reencoded(Δ9)::mCherry; cb-unc-119(+)] II
OD373	unc-119(ed3) III; ltsi9 [pOD831/pJE120; Pknl-1::KNL-1 reencoded(RRASA)::mCherry; cb-unc-119(+)] II
OD375	unc-119(ed3) III; ltsi11 [pOD832/pJE121; Pknl-1::KNL-1 reencoded(SAAA)::mCherry; cb-unc-119(+)] II
OD388	unc-119(ed3) III; ltsi1 [pOD809/pJE110; Pknl-1::KNL-1 reencoded::mCherry; cb-unc-119(+)] II; ruls32 [pAZ132; pie-1/GFP::his-58; unc-119(+)] III; ddls6 [pie-1/GFP::tbg-1; unc-119(+)] V
OD431	unc-119(ed3) III; ltsi16 [pOD930/pJE156; Pknl-1::KNL-1 reencoded(4A)::mCherry; cb-unc-119(+)] II; ruls32 [pAZ132; pie-1/GFP::his-58; unc-119(+)] III; ddls6 [pie-1/GFP::tbg-1; unc-119(+)] V
OD432	unc-119(ed3) III; ltsi18 [pOD931/pJE157; Pknl-1::KNL-1 reencoded(Δ9)::mCherry; cb-unc-119(+)] II; ruls32 [pAZ132; pie-1/GFP::his-58; unc-119(+)] III; ddls6 [pie-1/GFP::tbg-1; unc-119(+)] V
OD389	unc-119(ed3) III; ltsi9 [pOD831/pJE120; Pknl-1::KNL-1 reencoded(RRASA)::mCherry; cb-unc-119(+)] II; ruls32 [pAZ132; pie-1/GFP::his-58; unc-119(+)] III; ddls6 [pie-1/GFP::tbg-1; unc-119(+)] V
OD390	unc-119(ed3) III; ltsi11 [pOD832/pJE121; Pknl-1::KNL-1 reencoded(SAAA)::mCherry; cb-unc-119(+)] II; ruls32 [pAZ132; pie-1/GFP::his-58; unc-119(+)] III; ddls6 [pie-1/GFP::tbg-1; unc-119(+)] V
OD391	unc-119(ed3) III; ltsi1 [pOD809/pJE110; Pknl-1::KNL-1 reencoded::mCherry; cb-unc-119(+)] II; lts52 [pOD379; pie-1/GFP::Y69A2AR.30; unc-119(+)]
OD486	unc-119(ed3) III; ltsi16 [pOD930/pJE156; Pknl-1::KNL-1 reencoded(4A)::mCherry; cb-unc-119(+)] II; lts52 [pOD379; pie-1/GFP::Y69A2AR.30; unc-119(+)]
OD501	unc-119(ed3) III; ltsi18 [pOD931/pJE157; Pknl-1::KNL-1 reencoded(Δ9)::mCherry; cb-unc-119(+)] II; lts52 [pOD379; pie-1/GFP::Y69A2AR.30; unc-119(+)]
OD392	unc-119(ed3) III; ltsi9 [pOD831/pJE120; Pknl-1::KNL-1 reencoded(RRASA)::mCherry; cb-unc-119(+)] II; lts52 [pOD379; pie-1/GFP::Y69A2AR.30; unc-119(+)]
OD393	unc-119(ed3) III; ltsi11 [pOD832/pJE121; Pknl-1::KNL-1 reencoded(SAAA)::mCherry; cb-unc-119(+)] II; lts52 [pOD379; pie-1/GFP::Y69A2AR.30; unc-119(+)]
OD398	unc-119(ed3) III; ltsi14 [pOD857/pJE132; Pknl-1::KNL-1 reencoded(RRASA-SAAA)::mCherry; cb-unc-119(+)] II
OD476	unc-119(ed3) III; ltsi46 [pOD1040/pJE174; Pknl-1::KNL-1 reencoded(4A-RRASA)::mCherry; cb-unc-119(+)] II
OD402	unc-119(ed3) III; ltsi14 [pOD857/pJE132; Pknl-1::KNL-1 reencoded(RRASA-SAAA)::mCherry; cb-unc-119(+)] II; ruls32 [pAZ132; pie-1/GFP::his-58; unc-119(+)] III; ddls6 [pie-1/GFP::tbg-1; unc-119(+)] V
OD483	unc-119(ed3) III; ltsi46 [pOD1040/pJE174; Pknl-1::KNL-1 reencoded(4A-RRASA)::mCherry; cb-unc-119(+)] II; ruls32 [pAZ132; pie-1/GFP::his-58; unc-119(+)] III; ddls6 [pie-1/GFP::tbg-1; unc-119(+)] V
OD108	unc-119(ed3) III; lts52 [pOD379; pie-1/GFP::Y69A2AR.30; unc-119(+)]
OD110	unc-119(ed3) III; lts52 [pOD379; pie-1/GFP::Y69A2AR.30; unc-119(+)] II; lts37 [pAA64; pie-1/mCherry::his-58; unc-119(+)] IV
VC2787	(+/mT1 II; knl-1(ok3457)/mT1[dpv-10(e128)] III) – source strain for KNL-1Δ
EG4322	unc-119(ed3) III; ttTi5605 II – source for KNL-1 <sup>RR</sup> ::mCherry transgenic strains

Table S4. dsRNAs used in this study

Gene no.	Name	Concentration	Oligonucleotide no. 1	Oligonucleotide no. 2	Template
		mg/ml			
C02F5.1	knl-1	3.1	5'-ATAAACCTCACTAAAGGAATCT- CGAACTCACCGAAATGTC-3'	5'-TAATACGACTCACTATAGGTCA- CAAACTTGGAAAGCCGCTG-3'	cDNA
F59E12.2	zyg-1	2.6	5'-ATAAACCTCACTAAAGGTG- GACGGAAATCAACGAT-3'	5'-TAATACGACTCACTATAGGAAC- GAAATTCCCTTGAGCTG-3'	cDNA
Y69A2AR.30	mdf-2	2.2	5'-TAATACGACTCACTATAGGGAGA- CCACACGGATGAAAGACACAA- AACG-3'	5'-TAATACGACTCACTATAGGGAGACCAC- GTGAAGTACGCTGAGAATGAG-3'	cDNA
F29F11.6	gsp-1	3.8	5'-TAATACGACTCACTATAGGTGTC- GAACGATGGAGATTAA-3'	5'-ATAAACCTCACTAAAGGAATGAGTG- CAGCAATTGGAAAG-3'	cDNA
F56C9.1	gsp-2	3.9	5'-TAATACGACTCACTATAGGTG- GACGTAGAAAAGCTAATC-3'	5'-ATAAACCTCACTAAAGGGATGATG- GCGGCAACTGGCAGGCAG-3'	cDNA

## Reference

Hurley, T.D., J. Yang, L. Zhang, K.D. Goodwin, Q. Zou, M. Cortese, A.K. Dunker, and A.A. DePaoli-Roach. 2007. Structural basis for regulation of protein phosphatase 1 by inhibitor-2. *J. Biol. Chem.* 282:28874–28883.